

Critical points of Potts and $O(N)$ models from eigenvalue identities in periodic Temperley-Lieb algebras

Jesper Lykke Jacobsen^{1,2}

¹LPTENS, École Normale Supérieure – PSL Research University, 24 rue Lhomond, F-75231 Paris Cedex 05, France

²Sorbonne Universités, UPMC Université Paris 6, CNRS UMR 8549, F-75005 Paris, France

E-mail: `jesper.jacobsen@ens.fr`

Abstract.

In previous work with Scullard, we have defined a graph polynomial $P_B(q, T)$ that gives access to the critical temperature T_c of the q -state Potts model defined on a general two-dimensional lattice \mathcal{L} . It depends on a basis B , containing $n \times m$ unit cells of \mathcal{L} , and the relevant root $T_c(n, m)$ of $P_B(q, T)$ was observed to converge quickly to T_c in the limit $n, m \rightarrow \infty$. Moreover, in exactly solvable cases there is no finite-size dependence at all.

In this paper we show how to reformulate this method as an eigenvalue problem within the periodic Temperley-Lieb algebra. This corresponds to taking $m \rightarrow \infty$ first, so that the bases B are semi-infinite cylinders of circumference n . The limit implies faster convergence in n , while maintaining the n -independence in exactly solvable cases. In this setup, $T_c(n)$ is determined by equating the largest eigenvalues of two topologically distinct sectors of the transfer matrix. Crucially, these two sectors determine the same critical exponent in the continuum limit, and the observed fast convergence is thus corroborated by results of conformal field theory.

We obtain similar results for the dense and dilute phases of the $O(N)$ loop model, using now a transfer matrix within the dilute periodic Temperley-Lieb algebra.

Compared with our previous study, the eigenvalue formulation allows us to double the size n for which $T_c(n)$ can be obtained, using the same computational effort. We study in details three significant cases: (i) bond percolation on the kagome lattice, up to $n_{\max} = 14$; (ii) site percolation on the square lattice, to $n_{\max} = 21$; and (iii) self-avoiding polygons on the square lattice, to $n_{\max} = 19$. Convergence properties of $T_c(n)$ and extrapolation schemes are studied in details for the first two cases. This leads to rather accurate values for the percolation thresholds: $p_c = 0.524\,404\,999\,167\,439(4)$ for bond percolation on the kagome lattice, and $p_c = 0.592\,746\,050\,792\,10(2)$ for site percolation on the square lattice.

1. Introduction

The question what makes a two-dimensional lattice model amenable to exact solution has attracted considerable attention within the field of statistical mechanics. Most,

but not all, solutions have been found by the technique of integrability, in which the commutativity of an infinite family of transfer matrices is ensured by requiring the Boltzmann weights to solve a set of cubic functional relations, known as the Yang-Baxter equations [1].

Recent work has focussed on a construction called discrete holomorphicity (DH), in which suitable correlation functions are required to satisfy a discrete version of the Cauchy-Riemann equations [2]. This leads to linear relations among the Boltzmann weights, that express the conservation of certain non-local currents in an associated quantised affine algebra [3, 4]. The appropriate discretely holomorphic observables have been defined for several types of models, including Ising and Z_N models [5], loop models of the Potts [6] and $O(N)$ types [7], the chiral Potts model [8], and more exotic models involving multi-coloured loops [9].

In a series of papers with C.R. Scullard [10, 11, 12] we have defined a topologically weighted graph polynomial for Potts and site percolation problems, having properties that are somewhat reminiscent of those found in the DH approach. This polynomial P_B depends on the Boltzmann weights of the degrees of freedom living within a “basis” B , by which we mean a small repeating part of the lattice. The main similarity of the graph polynomial approach with DH is, that when a set of Boltzmann weights corresponding to an exact solution is inserted, it produces a root of P_B , independently of the size of B . In particular, when this size-independence is observed, it can be seen as heuristic evidence that we have found an exact solution. An important difference with DH is that the graph polynomial is defined as a partition function (albeit with some topological weighting of configurations), unlike the discretely holomorphic observables that take the form of correlation functions.

The graph polynomial method is also practically useful when the model is not exactly solvable. Given a fixed set of physical coupling constants, let us denote by $P_B(T)$ the evaluation of P_B with Boltzmann weights corresponding to the temperature T . It is then observed [10, 11, 12, 13] that the root T_B —that is, a solution of $P_B(T_B) = 0$ —converges very quickly towards the critical temperature T_c , upon increasing the size of B . This extends to models possessing several critical points [10], and even to inhomogeneous models with quenched bond disorder (spin glasses) [14].

The property of P_B just mentioned can then be used as a numerical tool for determining T_c very accurately. This was pursued extensively in [13] for the Potts model defined on all Archimedean lattices, their duals and their medials, as well as for site percolation on selected lattices (Archimedean and dual Archimedean lattices having only cubic and quartic vertices).

The purpose of this article is to enhance the efficiency of this method, and to place it in a larger perspective by making contact with a number of existing theoretical constructions. To this end, we consider bases B consisting of $n \times m$ unit cells of the lattice \mathcal{L} on which the model is defined. According to [11, 12], P_B is defined by endowing B with doubly periodic boundary conditions and imposing a certain topological weighting of each configuration. The key idea in the present paper is then to take the $m \rightarrow \infty$

limit first, so that the bases effectively become semi-infinite cylinders of circumference n . This transforms the criterion $P_B(T_B) = 0$ into an equality between eigenvalues of two topologically distinct sectors of the corresponding transfer matrix. These eigenvalue problems can then be solved—analytically for small bases, and numerically for larger ones—within the framework of the periodic Temperley-Lieb algebra [13].

This construction has several advantages. First, it makes the computation of $T_B = T_c(n)$ numerically much more efficient—allowing basically for doubling the size n attainable, with respect to the previous approach [13]—while maintaining the crucial feature that $T_c(n)$ has no n -dependence at all when the model is exactly solvable. Second, it makes useful contact with both the transfer matrix formalism and with conformal field theory (CFT), allowing for a better understanding of the method. Third, it extends the applicability of the method beyond Potts and site percolation problems [13]. In particular, we shall show how to adopt it to $O(N)$ loop models, in both the dense and dilute phases, in which case the underlying algebra is the dilute periodic Temperley-Lieb algebra. Fourth, since twice as many values $T_c(n)$ are available for a given problem, the finite-size scaling (FSS) behaviour can be studied much more carefully, and we can devise extrapolation schemes which are more efficient and reliable than the Bulirsch-Stoer acceleration of convergence employed in [13].

We illustrate all these aspects by applying the method to three significant unsolved problems, which in the past have each served as benchmarks within their respective category:

- (i) Bond percolation on the kagome lattice. This model has been the subject of a long-standing debate, since Wu's ingenious 1979 conjecture for the percolation threshold $p_c^{\text{Wu}} = 0.524\,429\,717 \dots$ [15]. This conjecture was however proved incorrect, both by subsequent numerical work [16], among which $p_c = 0.524\,404\,99(2)$ [17] appears to be the most precise value to this date, and—maybe on a more fundamental level—by the observation [10] that Wu's conjecture is exactly the outcome of the graph polynomial method with the smallest possible 1×1 basis (containing 6 edges). The previous graph polynomial method [13] gave $p_c = 0.524\,404\,999\,173(3)$, a result which we can now improve to

$$p_c = 0.524\,404\,999\,167\,439(4). \quad (1)$$

This exemplifies the first and fourth points made above, revealing in particular that the error bar of [13] was slightly underestimated.

- (ii) Site percolation on the square lattice. This renowned problem is unsolved essentially because the four-regular square-lattice hypergraph is not selfdual. The percolation threshold is in this case given by $p_c = 0.592\,746\,05(3)$ from numerical simulations [17], and by $p_c = 0.592\,746\,01(2)$ from the previous graph polynomial method [13]. We here improve this value to

$$p_c = 0.592\,746\,050\,792\,10(2). \quad (2)$$

- (iii) Self-avoiding polygons (SAP) on the square lattice. This is the polymer ($N \rightarrow 0$) limit of a dilute $O(N)$ loop model on the square lattice, in which each vertex

can be visited at most once by the polygon. There is a fugacity z per monomer, and no bending rigidity. This model has been investigated extensively by exact enumeration techniques [18, 19, 20]. The best known critical monomer fugacity is $z_c = 0.379\,052\,277\,752(3)$ [21]. We have obtained for this problem values of $z_c(n)$ up to $n_{\max} = 19$. While the extrapolation of these data is compatible with—and more precise than—the result of [21], we defer the discussion of extrapolations to a subsequent paper in which several numerical approaches to the SAP problem will be compared [22].

The paper is organised as follows. In section 2 we review the definition of the graph polynomial for the q -state Potts model. The transfer matrix formalism, to be used extensively in this paper, is set up in section 3. Section 4 discusses the $m \rightarrow \infty$ limit that leads to the eigenvalue method for the Potts model. Using a few implementational tricks (see section 5), we can then go on to determine the critical thresholds $p_c(n)$ for two selected percolation problems in section 6. The finite-size scaling behaviour of $p_c(n)$ is discussed in section 7. This leads to a powerful extrapolation scheme that provides the numerical values of $p_c = \lim_{n \rightarrow \infty} p_c(n)$ given in the abstract. Examining the relation of the eigenvalue method to conformal field theory, in section 8, enables us to generalise it to other representations (see section 9) and other models. In particular, section 10 sets up the method for the $O(N)$ model, and discusses its relation with exactly solvable models. The application to the SAP problem is also provided there. Finally, section 11 contains a few concluding remarks and perspectives for further investigations.

2. Graph polynomial

We first briefly review the definition of the graph polynomial for the case of the Potts model [10]. To set the scene for the eigenvalue method, we pay special attention to the ameliorations of computational complexity that were obtained in [12, 13].

Given a connected graph $G = (V, E)$ with vertex set V and edge set E , the partition function Z of the q -state Potts model [23] can be defined as [24]

$$Z = \sum_{A \subseteq E} v^{|A|} q^{k(A)}, \quad (3)$$

where $|A|$ denotes the number of edges in the subset A , and $k(A)$ is the number of connected components (including isolated vertices) in the subgraph $G_A = (V, A)$. The temperature variable is denoted $v = e^K - 1$, where K is the reduced interaction energy (including the inverse temperature) between adjacent q -component spins. In the representation (3) one can formally allow both q and v to take arbitrary real values. The special case of bond percolation is obtained by setting $q = 1$ and choosing the probability of an open bond as $p = \frac{v}{1+v}$.

The definition of the graph polynomial $P_B(q, v)$ made initially in [10] was in terms of a deletion-contraction principle, whose validity it well-known for the partition function itself. The subsequent work [12] provided an alternative definition that better reveals the

topological content of $P_B(q, v)$. We henceforth suppose that G is an infinite, regular, two-dimensional lattice \mathcal{L} . We define a basis B to be a finite subgraph of \mathcal{L} that produces all of \mathcal{L} upon application of an appropriate infinite set of translations that we call the embedding. The definition made in [12] is then in terms of conditioned partition functions, similar to (3), that are defined on a graph $G = (V, E)$ which is equal to the basis B :

$$P_B(q, v) = Z_{2D} - qZ_{0D}. \quad (4)$$

Here Z_{0D} is the sum over edge subsets $A \subseteq E$ such that all connected components (clusters) in the subgraph $G_A = (V, A)$ have trivial homotopy (i.e., are contractible to a point) upon endowing B with toroidal boundary conditions, whilst Z_{2D} corresponds to clusters that wrap both periodic directions. Note that the terms in Z_{1D} , corresponding to clusters wrapping one but not the other periodic direction, do not appear in (4).

From a computational point of view, the contraction-deletion algorithm described in [10] has time and memory requirements that grow like $2^{|E|}$, where $|E|$ is the number of edges in B . In practice we shall be interested in bases that are $n \times m$ patterns of the least possible unit cell for B ; a multitude of examples was given throughout [13]. For a regular lattice \mathcal{L} one has $|E| = k_{\mathcal{L}}nm$, and for Archimedean lattices with the square embedding considered in [13], the proportionality constant $k_{\mathcal{L}}$ ranges from 4 (square lattice) to 9 (three-twelve and cross lattices); see Table 3 of [13] for details. In the transfer matrix algorithm of [12] the growth in time and memory is only like $4^{2(n+m)}$, where $2(n+m)$ corresponds to the perimeter (number of terminals) of B , that is, the number of vertices shared with translated copies of B within the embedding. Finally, Ref. [13] provided an improved transfer matrix within the periodic Temperley-Lieb algebra in which one of the periodic boundary conditions on B was imposed “on the fly”; this is shown in Figure 3 of [13]. As a result, the exponential growth was reduced to $4^{2\min(n,m)}$.

In practical computations, one typically takes $m = n$, and so the computational effort is $2^{k_{\mathcal{L}}n^2}$ in [10], 256^n in [12], and 16^n in [13]. Accordingly, the maximum value of n that could be obtained for the Archimedean lattices was improved from $n_{\max} = 2$ in [10] to $n_{\max} = 4$ in [12], and further to $n_{\max} = 7$ in [13].

In this paper we show how to take the limit $m \rightarrow \infty$, so that the basis B becomes a semi-infinite cylinder of circumference n unit cells of \mathcal{L} . The roots of $P_B(q, v)$ in that limit can then be computed by solving an eigenvalue problem in the periodic Temperley-Lieb algebra. The corresponding transfer matrix then acts on only n terminals, and time and memory requirements reduce to 4^n . Accordingly, the computations can now be taken to $n_{\max} = 14$ for the Potts model on the Archimedean lattices. We shall illustrate this below, by computing the bond percolation threshold on the kagome lattice to high precision. Other values of q , and other lattices, are obviously also of interest, but a more systematic investigation will be reported separately [25].

3. Transfer matrix

We shall refer to (4) as the Fortuin-Kasteleyn (FK) representation of $P_B(q, v)$. Each connected component in the subgraph $G_A = (V, A)$ will be called an FK cluster. As in [13], we shall need an equivalent formulation in terms of a loop model [26] defined on the medial lattice $\mathcal{M}(B)$. We now review the salient points leading to the definition of the transfer matrix in the loop representation, as well as the connectivity states that it acts on.

The correspondence between FK clusters and loops can be depicted graphically as follows:



Here $e \equiv (ab) \in E$ is an edge of G , and the left (resp. right) picture represents the situation where $e \in A$ (resp. $e \notin A$). The equivalent loops (shown in red colour) live on $\mathcal{M}(B)$; they bounce off the edge subset A and cut through its complement $E \setminus A$.

To turn this local equivalence into a global one, one uses the Euler relation for a planar graph to rewrite the partition function (3) in the loop representation as [26]

$$Z = q^{|V|/2} \sum_{A \subseteq E} x^{|A|} n_{\text{loop}}^{\ell(A)}, \quad (6)$$

where $x = v/\sqrt{q}$, and $\ell(A)$ denotes the number of closed loops induced by the configuration A . The loop fugacity is $n_{\text{loop}} = \sqrt{q}$. We shall use the parameters (q, v) and (n_{loop}, x) interchangeably.

The loops on $\mathcal{M}(B)$ provide a representation of the Temperley-Lieb (TL) algebra. Supposing the direction of “time” propagation in (5) to be upwards, the left (resp. right) picture corresponds to the action of the identity operator \mathbf{I} (resp. the TL generator \mathbf{E}_i) on the two adjacent strands, labelled i and $i + 1$ from left to right. We then have the relations [27]

$$\begin{aligned} \mathbf{E}_i^2 &= n_{\text{loop}} \mathbf{E}_i, \\ \mathbf{E}_i \mathbf{E}_{i \pm 1} \mathbf{E}_i &= \mathbf{E}_i, \\ \mathbf{E}_i \mathbf{E}_j &= \mathbf{E}_j \mathbf{E}_i \quad \text{for } |i - j| > 1, \end{aligned} \quad (7)$$

which may be proved graphically by gluing several diagrams in the form (5) on top of one another.

The partition function (6) for a basis of size $n \times m$ can be computed within the TL algebra as shown in Figure 1. The operator $\check{\mathbf{R}}_i$ is here an element of the TL algebra built out of generators \mathbf{E}_j with $j \in \{i, i + 1, i + 2\}$, acting on connectivity states consisting of $2n$ strands, labelled $0, 1, \dots, 2n - 1$. The particular arrangement of Figure 1 is called a four-terminal representation of B [13]. Further details of this construction and explicit expressions for $\check{\mathbf{R}}_i$ for all Archimedean lattices can be found in [13].

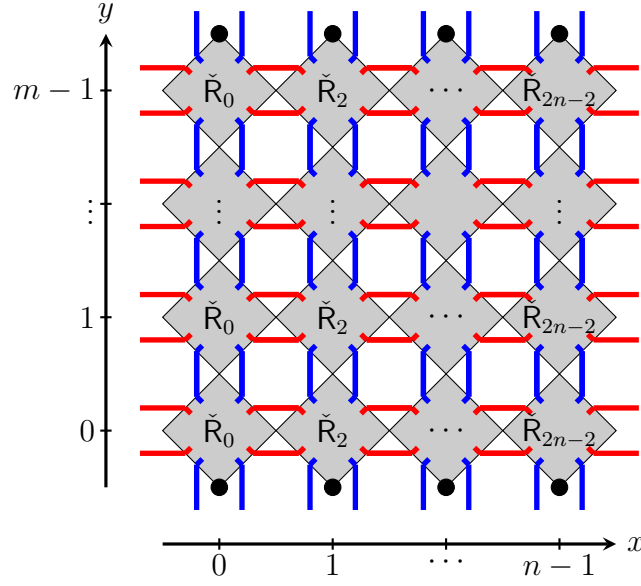


Figure 1. Basis of size $n \times m$ in the loop representation. Terminals of the basis are shown as black circles, and periodic boundary conditions have been imposed horizontally. The auxiliary and quantum spaces, shown in red and blue colour respectively, sustain loops which are acted upon by an \check{R}_i -matrix inside each grey square.

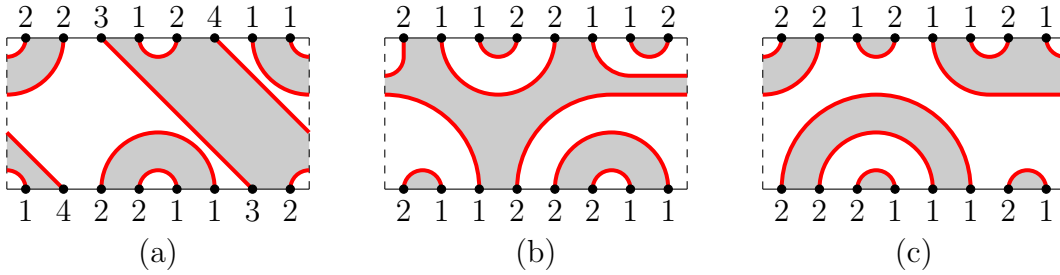


Figure 2. Three examples of connectivity states for $n = 4$. The numbers along the two time slices provide a canonical coding of the connectivity state. Loops are shown as red solid lines. The corresponding FK clusters live in the areas shaded in grey, whilst the dual FK clusters live in the white areas.

A few examples of connectivity states are shown in Figure 2. The states are defined on two time slices (top and bottom), that describe the configuration of the system between vertical positions $y = -1/2$ (bottom) and $y = t - 1/2$ (top), after any internal loop has been replaced by the factor n_{loop} , upon application of (7). The transfer matrix that propagates the system from “time” t to $t + 1$ is then given by the product of all \check{R}_i operators within a row, where the periodic horizontal boundary conditions are implemented by tracing over the auxiliary spaces (shown in red colour in Figure 1).

Let us now be more specific about which variant of the TL algebra we actually need. The choice of periodic boundary conditions in the horizontal direction means

that the standard TL algebra [27] (with generators E_i for $i = 0, 1, \dots, 2n - 2$) must be made periodic. In the resulting periodic TL algebra there is an extra generator E_{2n-1} that acts across the periodic boundary condition (i.e., between strands $2n - 1$ and 0). This algebra is however infinite-dimensional, and two modifications (algebra quotients) must be applied in order to make it finite-dimensional again. First, any loop of non-trivial homotopy (i.e., that winds around the periodic horizontal direction while being detached from the top and bottom time slices) must be replaced by a factor n_{wind} . Second, loop segments connecting the two time slices are only considered according to which points they connect, and not how many turns they make around the periodic x -direction. The corresponding convention in Figure 2 is that among such connecting segments, the one that is leftmost in the top time slice (i.e., that carries the label ‘3’ in Figure 2) is required not to cross the periodic direction. Note however that we still need to distinguish whether loop segments that connect a given time slice to itself crosses the periodic direction or not. With these modifications, the corresponding algebraic object is known as the *augmented Jones-Temperley-Lieb algebra*; see section 3.1 of [28] for more details.

In order to discuss further the states in Figure 2, we call *arc* a loop segment that connects two points within the same time slice, and *string* a loop segment that connects points on different time slices. The number of strings $s = 2k$ is always even. When $s > 0$ there are k FK clusters (and also k dual FK clusters) connecting the top and bottom time slices. A state can be turned into a pair of “reduced states” by cutting the s strings (if any) between the bottom and top time slices; each reduced state is then associated with only one time slice. Conversely, a pair of reduced states can be glued along the strings so as to form a “complete” state. This gluing can be done in k inequivalent ways, corresponding to cyclic rotates of the strings of one of the reduced states, in units of two (otherwise the distinction between FK clusters and dual FK clusters would fail to be respected). The $s = 0$ reduced states consist only of arcs and can be either *closed* (all FK clusters are bounded away from infinity) or *open* (at least one FK cluster is not bounded). For example, Figure 2b shows a state consisting of two open reduced states, whilst Figure 2c depicts a pair of closed reduced states. Note that each reduced $s = 0$ state can be conveniently coded in a binary convention where the code 1 (resp. 2) means a arc opening (resp. closing).

A subtlety particular to the computation of $P_B(q, v)$ arises because Z_{1D} does not appear in (4). We must therefore set $n_{\text{wind}} = 0$. This implies that the $s = 0$ states can only be gluings of two open reduced states, or of two closed reduced states. In other words, mixed gluings are not allowed. We shall call such $s = 0$ states open or closed, respectively.

Below, in section 4, we shall expose our main argument for transforming the computation of $P_B(q, v)$ into an eigenvalue problem in the limit $m \rightarrow \infty$. On the level of the transfer matrix, this argument will imply an important simplification with respect to [13]. Namely, the eigenvalue problem can be solved by using only the top time slice, so that the transfer matrix acts only on reduced states. Moreover, only reduced

states without strings ($s = 0$) are needed—at least in the probabilistic regime $v > 0$ considered here. There is an equal number of open and closed reduced states, namely

$$\frac{1}{2} \binom{2n}{n} \sim 4^n \quad (8)$$

of each. (In the intermediate stages of the computation, when n_{aux} auxiliary spaces are open, simply replace n by $n + n_{\text{aux}}$). The gain of performance of the present method is largely due to the fact that (8) is much less than the number of “complete” states, which grows like $\sim 16^n$; see Eq. (14) of [13].

4. Taking the $m \rightarrow \infty$ limit

After these preliminaries, we now consider computing $P_B(q, v)$ from (4) for an $n \times m$ basis with finite n and $m \gg n$; see Figure 1. In this limit, B has the geometry of a semi-infinite cylinder, which naturally suggests an interpretation in terms of the eigenvalues of a transfer matrix.

When ordering the states according to a decreasing number of strings s , the transfer matrix T of section 3, with two time slices, has a lower block-triangular structure (the blocks being indexed by s), since under the time evolution the number of strings cannot increase. Its eigenvalues are therefore the union of the eigenvalues of each block on the diagonal, i.e., each eigenvalue can be characterised by the corresponding number of strings s . We denote these blocks by $T^{(s)}$. Moreover, the $s = 0$ block is a direct sum of two terms, T_{open} and T_{closed} , corresponding to a pair of open (resp. a pair of closed) reduced states. This is so precisely because contributions to Z_{1D} are excluded from (4), implying that loops winding around the cylinder carry the weight $n_{\text{wind}} = 0$. So, as far as the eigenvalue problem is concerned, we can replace T by the direct sum

$$\tilde{T} = \bigoplus_{k=1}^n T^{(s=2k)} \oplus T_{\text{open}} \oplus T_{\text{closed}}. \quad (9)$$

The modified transfer matrix \tilde{T} thus has the same spectrum as T , and moreover it conserves the quantum number s and, for $s = 0$, also the additional quantum number “open” and “closed”. Since \tilde{T} acts on the top time slice, and unlike T it cannot decrease s , it is unable to change the bottom reduced state. In other words, each of the direct summands $T^{(s)}$ in (9) is in turn a direct sum of N_s of identical blocks, with N_s being the number of reduced states with s strings corresponding to the bottom time slice. Up to multiplicities of the eigenvalues, it therefore suffices to consider the action of (9) on the reduced states corresponding to the top time slice. In other words, the set of eigenvalues of T (that acts on “complete” states with two time slices) is the union of eigenvalues of $T^{(s)}$, T_{open} and T_{closed} , each restricted to act only on the set of reduced states.†

We are interested in models with $q > 0$, and let us assume further that we are in the ferromagnetic regime, $v > 0$. All Boltzmann weights are therefore positive, and

† A similar argument has been given in [29, 30].

by the Perron-Frobenius theorem each summand in the decomposition (9) therefore has a unique, positive largest eigenvalue that we denote $\Lambda^{(s)}$ for $s > 0$, respectively Λ_{open} and Λ_{closed} for $s = 0$. These eigenvalues obviously depend on the size n , and on the parameters (q, v) . It follows from the cylinder geometry and the probabilistic assumption $v > 0$ that the eigenvalues are ordered

$$\Lambda_{\text{open}}, \Lambda_{\text{closed}} > \Lambda^{(2)} > \Lambda^{(4)} > \dots > \Lambda^{(2n)}. \quad (10)$$

Moreover, each of the terms in (4), Z_{2D} and Z_{0D} , must behave as $\sim \Lambda^m$, where Λ is one of the above eigenvalues. By (10) the dominant contributions come from Λ_{open} and Λ_{closed} . Since Z_{2D} (resp. Z_{0D}) corresponds to an FK cluster (resp. a dual FK cluster) spanning the length of the cylinder, we must have

$$Z_{2D} \sim (\Lambda_{\text{open}})^m, \quad (11)$$

$$Z_{0D} \sim (\Lambda_{\text{closed}})^m. \quad (12)$$

Note that these clusters will also wind around the circumference of the cylinder, with probability 1 in the limit $m \rightarrow \infty$, since the number of strings is $s = 0$.

It is obvious that Λ_{open} and Λ_{closed} are both greater than unity, so Z_{2D} and Z_{0D} grow exponentially with m . If (4) is to have a (positive, unique) zero as a function of v —as is indeed observed [10, 12, 13]—there must exist some $v_c(n) > 0$ so that $\Lambda_{\text{open}} = \Lambda_{\text{closed}}$.

We can prove this statement as follows. For $v \gg 1$ the dominant contribution to (3) will be $A = E$, and hence $\Lambda_{\text{open}} > \Lambda_{\text{closed}}$ by direct computation. Conversely, for $v \ll 1$ the dominant contribution is $A = \emptyset$, whence $\Lambda_{\text{open}} < \Lambda_{\text{closed}}$. Since both terms in (4) grow exponentially in m , the factor of q is unimportant, and the intermediate value theorem implies our main result

$$P_B(q, v) = 0 \quad \Leftrightarrow \quad \Lambda_{\text{open}} = \Lambda_{\text{closed}}, \quad (13)$$

valid for a basis B of size $n \times m$, with n finite and $m \rightarrow \infty$.

We can therefore find the (unique) positive root, $v > 0$, of the graph polynomial for bases that are semi-infinite cylinders of circumference n by solving a simple eigenvalue problem over the $s = 0$ reduced states. Their number is given by (8) and grows as $\sim 4^n$, providing a substantial improvement over [13] in which Z_{2D} and Z_{0D} were computed by imposing complicated boundary conditions on a transfer matrix acting in the full set of states with dimension $\sim 16^n$.

In the remainder of this section we first illustrate the main result (13) in a few simple cases. We end by discussing the special role of exactly solvable models.

4.1. Square lattice with $n = 1$

Consider the four-terminal representation of the square lattice with $n = 1$. There are 3 reduced states which can be written $||$, $()$ and $)()$, where $|$ denotes a string, $()$ is an arc opening, and $)()$ is an arc closing. For the time being, we allow winding loops with weight n_{wind} . It is easy to see that in the basis $\{||, (), ()()\}$ the transfer matrix reads $T = T_2 T_1$

with

$$T_1 = \begin{bmatrix} 2x & 0 & 0 \\ x^2 & n_{\text{wind}}x^2 & 2x + n_{\text{loop}}x^2 \\ 1 & 2x + n_{\text{loop}} & n_{\text{wind}} \end{bmatrix}, \quad (14)$$

$$T_2 = \begin{bmatrix} 2x & 0 & 0 \\ 1 & n_{\text{wind}} & 2x + n_{\text{loop}} \\ x^2 & 2x + n_{\text{loop}}x^2 & n_{\text{wind}}x^2 \end{bmatrix}, \quad (15)$$

where we recall that $n_{\text{loop}} = \sqrt{q}$ and $x = v/\sqrt{q}$. Setting $n_{\text{wind}} = 0$ we obtain

$$T = \begin{bmatrix} 4x^2 & 0 & 0 \\ n_{\text{loop}} + 4x & (n_{\text{loop}} + 2x)^2 & 0 \\ x^4(4 + n_{\text{loop}}x) & 0 & x^2(2 + n_{\text{loop}}x)^2 \end{bmatrix}, \quad (16)$$

which is indeed a lower block-triangular matrix, corresponding to the blocks $s = 2$, $s = 0$ (closed), and $s = 0$ (open). Here, each of the blocks have dimension 1. The (dominant) eigenvalues read

$$\Lambda^{(2)} = 4x^2, \quad \Lambda_{\text{closed}} = (n_{\text{loop}} + 2x)^2, \quad \Lambda_{\text{open}} = x^2(2 + n_{\text{loop}}x)^2. \quad (17)$$

For $n > 0$ and $x > 0$ the ordering (10) is respected indeed.

To investigate the result (13) we remark that

$$\Lambda_{\text{open}} - \Lambda_{\text{closed}} = n_{\text{loop}}(x^2 - 1)(n_{\text{loop}}x^2 + 4x + n_{\text{loop}}) \quad (18)$$

is proportional to the graph polynomial $P_B(q, v) = (v^2 - q)(q + 4v + v^2)$ for the $n \times m = 1 \times 1$ basis [10]. In this case, where all blocks are one-dimensional, it is obvious—and can be verified by explicit computations—that the relevant (i.e., positive) roots of $P_B(q, v)$ are independent of m . Note also that, despite of the assumption $v > 0$, this example actually correctly describes the phase diagram of the square-lattice Potts model both in the ferromagnetic ($v > 0$) and antiferromagnetic ($v < 0$) regimes, i.e., $\Lambda^{(2)}$ can simply be ignored.

4.2. Kagome lattice with $n = 1$

Consider next the kagome lattice with $n = 1$. Setting $n_{\text{wind}} = 0$ from the outset and considering only the $s = 0$ states $\{(), ()\}$ we find that T is a diagonal 2×2 matrix with eigenvalues

$$\Lambda_{\text{closed}} = (n_{\text{loop}} + 2x)(n_{\text{loop}}^2 + 4n_{\text{loop}}x + 6x^2 + 2n_{\text{loop}}x^3), \quad (19)$$

$$\Lambda_{\text{open}} = x^2(2n_{\text{loop}} + 12x + 13n_{\text{loop}}x^2 + 6n_{\text{loop}}^2x^3 + n_{\text{loop}}^3x^4). \quad (20)$$

The difference $\Lambda_{\text{open}} - \Lambda_{\text{closed}}$ is proportional to

$$P_B(q, v) = v^6 + 6v^5 + 9v^4 - 2qv^3 - 12qv^2 - 6q^2v - q^3, \quad (21)$$

which is the graph polynomial for the 1×1 basis. Back in 1979, Wu [15] conjectured this expression to be the exact critical manifold of the kagome-lattice Potts model, but

m	p_c
1	0.524429717521274793546879681534455071620567416578664793997510
2	0.524406723188231819143234479992589885410333714096742273226669
4	0.524406058417857416583229008103273638077164830301055000364284
8	0.524406057896062955151905518860778390220248322088553687927465
16	0.524406057896062634245378836787730760263849423348568828123454
32	0.524406057896062634245378836666345666792028877197553627352494
∞	0.524406057896062634245378836666345666792028877197553609980248

Table 1. Bond percolation threshold p_c on the kagome lattice using bases of size $2 \times m$ for various m .

our recent work [10, 12, 13] definitively established that this is only an approximation corresponding to the smallest possible choice of the basis B .

Once again the roots of $P_B(q, v)$ for all the $1 \times m$ bases are independent of m , because the blocks T_{open} and T_{closed} are one-dimensional.

4.3. Kagome lattice with $n = 2$

In Table 1 we show the estimates for the bond percolation threshold p_c obtained as the relevant roots of $P_B(1, v)$, with $p = v/(1 + v)$, for bases of size $n \times m$ with fixed $n = 2$ and varying m . The results for finite m were obtained from the algorithm of [13]. They are compared with the $m = \infty$ result obtained from (13) using the transfer matrix construction of the present paper.

As expected, the results converge rapidly to the $m = \infty$ limit, the rate of convergence being exponential in m . We also note that the $2 \times \infty$ result 0.524 406 057 \dots (i.e., the semi-infinite cylinder basis) is closer to the true percolation threshold $p_c = 0.524 404 999 \dots$ [13] than is the 2×2 result 0.524 406 723 \dots (i.e., the square basis). Taking $m \rightarrow \infty$ in the $2 \times m$ results is however far from “gaining one size”, since the 3×3 result is 0.524 405 172 \dots . These observations extend to arbitrary values of n .

4.4. Exactly solvable cases

It was shown in [13] that $P_B(q, v)$ factorises over the integers for the three-terminal lattices (square, triangular and hexagonal), and that in the Ising case $P_B(2, v)$ factorises for any lattice. In these factorisations, one or more “small” factors were observed to be independent of the size $n \times m$ of the basis, and their corresponding roots coincided with known exact solutions. In addition, a few sporadic cases were found in [13], mainly concerning $P_B(0, v)$, where a size-independent factorisation occurred, and it was conjectured that these cases would be exactly solvable.

Because of the m -independence of this factorisation result, it should still hold in the $m \rightarrow \infty$ limit. We therefore expect that $\Lambda_{\text{open}} - \Lambda_{\text{closed}}$ will factorise in exactly solvable cases, spawning an n -independent factor whose roots provide the exact critical points.

We have already seen this happen in (18), and we have verified by explicit computations that this is indeed so also for higher n and for other exactly solvable models.

5. Practical considerations

To take the study to larger sizes n , we have implemented numerically the computation of the eigenvalues Λ_{open} and Λ_{closed} that enter our main result (13). The transfer matrix T needs to be diagonalised in the sectors T_{open} and T_{closed} , and the first question to be settled is which is the most efficient technique for doing so.

We have seen that T can be written as a product of \check{R}_i operators, and these can in turn be written as product of the elementary operators

$$H_i = I + xE_i, \quad V_i = xI + E_i, \quad (22)$$

that add respectively a horizontal (or “space-like”) and a vertical (or “time-like”) edge to the lattice [13]. The operators H_i and V_i are very sparse, with at most two non-zero entries per column, so the computation of $w_2 = Tw_1$, where w_1 is a vector of dimension (8), can be done with time and memory requirements which are proportional to that dimension. This calls immediately for iterative diagonalisation techniques [31].

The method of choice within this category is the Arnoldi method. However, we shall need to compute the eigenvalues to high numerical precision (cf. Table 1), and we do not know of an implementation of the Arnoldi method which is compatible with arbitrary precision libraries. Moreover, we need only the largest eigenvalue in each of the sectors T_{open} and T_{closed} , so a very simple method should be sufficient for our purposes. We have therefore used the most naive scheme, the so-called power method, in which the operations $w_2 = Tw_1$ followed by $w_1 = w_2/||w_2||$ are iterated until $||w_2||$ and w_1 have converged to the largest eigenvalue of T and its corresponding eigenvector, respectively. To obtain convergence of the eigenvalue to 40-digit numerical precision, it turned out necessary to perform several hundreds of iterations, in particular for large sizes n .

The action of Temperley-Lieb generators on the reduced states was described in [13]. Since we have $s = 0$ there are significant simplifications. The insertion and removal of the $n_{\text{aux}} = 2$ auxiliary spaces (made necessary by the four-terminal representation of Figure 1) are handled exactly as in [13]. In our implementation the states are stored in a hash table, since we want to take full advantage of the fact that for some problems (like, for instance, site percolation on the square lattice) the number of states needed can be even less than (8).

Another major simplification of the eigenvalue method is that no complicated topological considerations—such as those made in section 3.7 of [13]—will be required in order to distinguish contributions to Z_{2D} and Z_{0D} in (4). To choose the sector, it suffices to start the iterative scheme with an initial vector v equal to one of the reduced states in the ‘open’ or ‘closed’ sector, respectively.

Considerations about efficiency are not limited to choosing the optimal numerical scheme for computing the eigenvalues. Once we can evaluate the function $f(v) =$

$\Lambda_{\text{open}} - \Lambda_{\text{closed}}$ for some value of the temperature variable v , we need also an efficient means of adjusting v to its critical value $v_0 \equiv v_c(n)$ satisfying $f(v_0) = 0$. Bracketing methods for finding zeros of a continuous function are numerically very stable, but rather slow. If we allow ourselves to compute derivatives, we can use instead the Newton-Raphson method, and more generally with k 'th order derivatives we can employ the k 'th order Householder method. The higher-order methods will in principle converge faster, but in practice the computation of high-order derivatives is numerically unstable, so some compromise must be found.

In practice we have found that the best result is provided by the second-order Householder method, with derivatives being computed by the symmetric difference method. Suppose we perform the computations in d -digit arithmetics (in practice we have taken $d = 40$). Let us set $\varepsilon = 10^{-d/2}$. Given some estimate v close to v_0 , one Householder iteration proceeds as follows. Make three evaluations of $f(v)$,

$$g_0 = f(v - \varepsilon), \quad g_1 = f(v), \quad g_2 = f(v + \varepsilon), \quad (23)$$

and apply the following formulae for the finite-difference derivatives:

$$f_0 = g_1, \quad f_1 = \frac{g_2 - g_0}{2\varepsilon}, \quad f_2 = \left(\frac{g_2 - g_1}{\varepsilon} - \frac{g_1 - g_0}{\varepsilon} \right) \varepsilon^{-1}. \quad (24)$$

We stress here that to achieve numerical stability, the order of operations has to be carefully respected when computing f_2 . Finally, the next approximation to v_0 is given by the second-order Householder formula

$$v_{\text{new}} = v - \frac{f_0 f_1}{(f_1)^2 - \frac{1}{2} f_0 f_2}. \quad (25)$$

Extensive tests of this method shows that it has the following nice properties:

- (i) After a few iterations, v converges to v_0 to full d -digit precision.
- (ii) If v is chosen sufficiently close to v_0 , the number of correct digits will double in each iteration.

The main computational effort obviously goes into the largest sizes n , and it is important in those cases to provide the best possible starting value v_{init} for v . Thanks to the scaling theory developed in section 7, we have been able to predict v_{init} so that $|v_{\text{init}} - v_0| < 10^{-15}$ or better. This means that we can attain our $d = 40$ digit goal in just two Householder iterations. In a few cases we have contented ourselves with just a single Householder iteration and a final precision of at least 30 digits.

6. Percolation thresholds on selected lattices

In this section we apply the eigenvalue method to two prominent sample problems which have been extensively studied in the past: site percolation on the square lattice, and bond percolation on the kagome lattice.

We stress that it would be straightforward to study also the Potts model for other values of $q \neq 1$, or to switch to any of the other lattices treated in [13]. To this end, it

suffices to change the \check{R}_i matrix to any of the explicit expressions given in [13], which is a matter of changing just a few lines of code. We shall however defer these extensions to a future study [25], and for the time being take the computations for the two problems mentioned as far as possible.

6.1. Site percolation on the square lattice

The \check{R} -matrix for site percolation on the square lattice is given by Eq. (76) in [13]:

$$\check{R}_i = E_{i+2}E_i + vE_{i+1}, \quad (26)$$

where we recall that $q = 1$ and the probability of an open bond is $p = \frac{v}{1+v}$. This \check{R} -matrix contains only two out of fourteen possible terms, so thanks to the use of hashing techniques only a subset of the reduced states will be used in the diagonalisation procedure (see sections 3.6 and 7.0 of [13] for more details).

The site thresholds were found on $n \times n$ square bases up to $n_{\max} = 11$ in [13]. Using the eigenvalue method we have obtained the thresholds on $n \times \infty$ bases up to $n_{\max} = 21$. These results are shown in Table 2. A comparison with Table 52 of [13] shows that the $10 \times \infty$ result is very close to the old 11×11 results, so having taken the $m \rightarrow \infty$ limit can be said, roughly speaking, to have “gained us one size” in this case.

It is obvious from Table 2 that there is agreement with the existing results for p_c on at least the first five digits. More digits can however be obtained by extrapolating the data, and this will be discussed in section 7.

6.2. Kagome lattice (3, 6, 3, 6)

The \check{R} -matrix for the Potts model on the kagome lattice is given by Eq. (29) of [13]:

$$\check{R}_i = H_{i+1}V_{i+2}V_iE_{i+1}V_{i+2}V_iH_{i+1}, \quad (27)$$

where the elementary operators H_i and V_i were defined in (22). We set $q = 1$ to obtain the corresponding bond percolation problem.

The bond thresholds were found on $n \times n$ square bases up to $n_{\max} = 7$ in [13]. From the eigenvalue method we have computed the thresholds on $n \times \infty$ bases up to $n_{\max} = 14$. Those results are shown in Table 3. The value $p_c(2)$ was already presented in Table 1.

It is immediately visible that the data in Table 3 converge faster than those in Table 2. The value of $p_c(n)$ with $n = 14$ agrees with p_c to eleven digits. Looking down the table we can also see that the central value for p_c given in Ref. [13] is a bit too high, and that the final extrapolated result is likely to be slightly below its lower error bound. We shall discuss this extrapolation in section 7.

7. Extrapolations

We shall now discuss the extrapolation of the data in Tables 2–3 in view of obtaining final values of the thresholds p_c which are as precise as possible.

n	$p_c(n)$
1	0.5244297175212747935468796815344550716205
2	0.5244060578960626342453788366663456667920
3	0.5244050922187183914064917102789956045159
4	0.5244050138823434506779249332748912013263
5	0.5244050026660985339974686380437997371046
6	0.5244050002521386411660652383853120094089
7	0.5244049995708026048576486896416033403853
8	0.5244049993387487061840419066777093506317
9	0.5244049992479802098067018389586796534330
10	0.5244049992084754512628552771194320896813
11	0.5244049991897559735118013090108129282307
12	0.5244049991802484437799696383468246717858
13	0.5244049991751328450538203030184876090453
14	0.524404999172242908087780703763
Ref. [17]	0.52440499 (2)
Ref. [13]	0.524404999173 (3)

Table 3. Bond percolation threshold p_c on the kagome lattice, as computed from $n \times \infty$ bases, and two previous results for p_c .

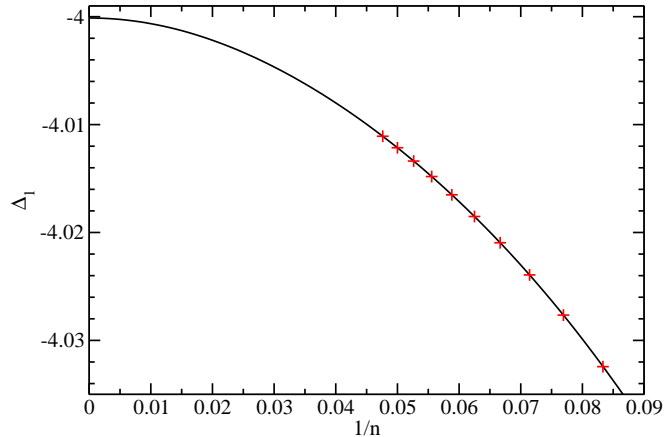


Figure 3. Determination of the first FSS exponent Δ_1 for site percolation on the square lattice.

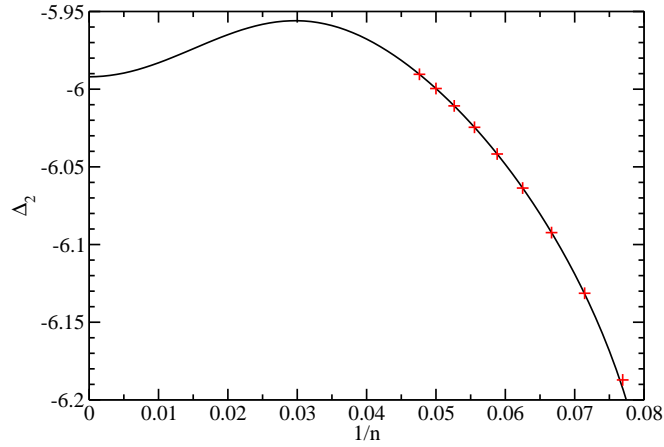


Figure 4. Determination of the second FSS exponent Δ_2 for site percolation on the square lattice.

In Figure 3 we show $\Delta_1(n)$ as a function of $1/n$. The data are very well fitted by a polynomial in $1/n^2$, and allowing for some freedom on the degree of the polynomial and the number of small- n points to be excluded from the fit, we arrive at the result

$$\Delta_1 = 4.0001(2). \quad (30)$$

This agrees well with the value $w = 4.03 \pm 0.01$ reported in section 7.2 of [13], which was found as the optimal choice for the FSS exponent entering the Bulirsch-Stoer algorithm. It appears inevitable to admit that $\Delta_1 = 4$ exactly.

We next form the sequence

$$p_4(n) = \frac{n^4 p_c(n) - (n-1)^4 p_c(n-1)}{n^4 - (n-1)^4} \quad (31)$$

in which the leading FSS term A_1/n^4 has been subtracted off (28). From this we form a sequence

$$\Delta_2(n) = \frac{\log(\delta p_4(n)) - \log(\delta p_4(n-1))}{\log(n) - \log(n-1)}, \quad (32)$$

which should now converge to the second FSS exponent Δ_2 . We plot $\Delta_2(n)$ against $1/n$ in Figure 4, along with a polynomial fit in $1/n^2$. This yields

$$\Delta_2 = 6.00(1). \quad (33)$$

and we henceforth admit that $\Delta_2 = 6$ exactly.

It is now obvious how to continue. In the next round we subtract $A_1/n^4 + A_2/n^6$ from (28) and seek to determine Δ_3 from the residue. Going through the same steps as above we find $\Delta_3 = 8.0(5)$, and we conjecture that $\Delta_3 = 8$.

The determinations of Δ_1 , Δ_2 and Δ_3 provide compelling evidence that $\Delta_k = 2(k+1)$ for any k . The precise FSS form then reads

$$p_c(n) = p_c + \sum_{k=1}^{\infty} \frac{A_k}{n^{2(k+1)}}. \quad (34)$$

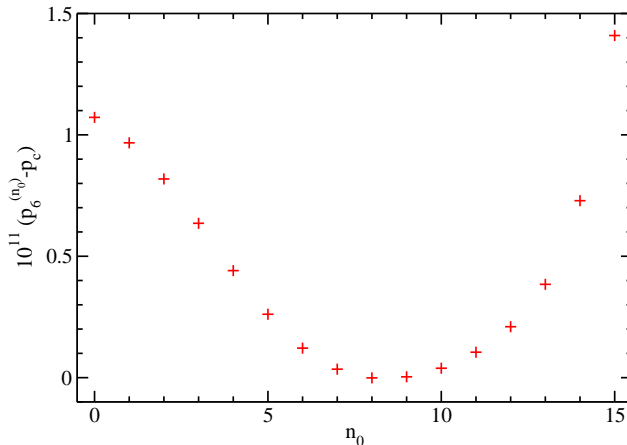


Figure 5. The estimators $p_6^{(n_0)}$ (in arbitrary units) plotted against n_0 .

We now show how to use this form to obtain a very precise extrapolation for the percolation threshold p_c .

Let n_{\max} denote the largest size for which we have been able to compute $p_c(n)$. In the present case we have $n_{\max} = 21$, as seen in Table 2. We first form a series of estimators $p_{M,L}$ in which the scaling form (34) is truncated at the $1/n^M$ term, and in which the data $p_c(n)$ is used up to a maximum size of $n = L$. In other words, we find the unique solution of the linear system

$$p_{M,L} + \left(\frac{A_1}{n^4} + \frac{A_2}{n^6} + \cdots + \frac{A_{M/2-1}}{n^M} \right) = p_c(n), \quad (35)$$

with $n = L + 1 - M/2, \dots, L - 1, L$. Second, for a fixed M , we form another series of estimators $p_M^{(n_0)}$ by fitting $p_{M,L}$ to the residual dependence predicted by (34), but eliminating from the fit the first n_0 possible values of L . That is, we find the unique solution of the linear system

$$p_M^{(n_0)} + \left(\frac{B_1}{n^{M+2}} + \frac{B_2}{n^{M+4}} + \cdots + \frac{B_{n_{\max}-n_0-1-M/2}}{n^{2(n_{\max}-n_0-1)}} \right) = p_{M,L}. \quad (36)$$

This is a fit on $n_{\max} - n_0 - M/2$ different values of L ranging from $1 + M/2 + n_0$ up to n_{\max} .

If we eliminate too few data points (i.e., take n_0 too small) when forming the estimators $p_M^{(n_0)}$, the result will be mediocre because it depends too much on the smallest sizes for which the FSS form (34) is dubious. On the other hand, if we eliminate too many data points (i.e., take n_0 too large) the result will again deteriorate because the fit has too few terms. We would expect an optimum in between these extremes.

In Figure 5 we show the variation of $p_M^{(n_0)}$ with n_0 in the case $M = 6$. For reasons of clarity, we actually plot the quantity $10^{11}(p_M^{(n_0)} - p_c)$, where p_c is our final value for the percolation threshold, but the units of the ordinate in the plot should really been thought of as arbitrary, since we have not determined p_c yet. We see that there is an extremum (minimum) at some intermediate value of n_0 , in agreement with the

M	Estimate
4	0.592746050791752
6	0.592746050792111
8	0.592746050792085
10	0.592746050792096
12	0.592746050792125
14	0.592746050792165
16	0.592746050792226

Table 4. Estimates $\frac{1}{2}(p_M^{(8)} + p_M^{(9)})$ for the site percolation threshold on the square lattice p_c .

above qualitative argument. Repeating the plot for other values of M (not shown), it is observed that the minimum becomes more shallow upon increasing M , at least up to a certain point beyond which the quality of the plot deteriorates due to a lack of points.

For any value of M in a reasonable range (namely $M = 4, 6, \dots, 16$) the minimum is found to occur for $n_0 = 8$ or $n_0 = 9$. The arithmetic mean of those two values of $p_M^{(n_0)}$ can thus be taken as a precise estimate for p_c . We show these mean values in Table 4 to 15 significant digits. They are seen to depend only very weakly on M in some intermediate range (say $M = 6, 8, 10, 12$) from which we can extract our final value and error bar for the percolation threshold:

$$p_c = 0.592\,746\,050\,792\,10(2). \quad (37)$$

7.2. Bond percolation on the kagome lattice

For bond percolation on the kagome lattice we again start by considering an FSS Ansatz of the form (28). It is immediately clear from the data that the leading FSS term does *not* correspond to the exponent $\Delta_1 = 4$, as was found for site percolation on the square lattice. To obtain a unified notation we therefore set $A_1 = 0$ in the kagome case, and call the leading FSS correction A_2/n^{Δ_2} .

Figure 6 shows estimates $\Delta_2(n)$ for this leading FSS exponent—extracted from the data $p_c(n)$ just as in (29)—, plotted against $1/n$. The accompanying fit is a second-order polynomial in $1/n$, and this and similar fits lead to the value

$$\Delta_2 = 6.00(5). \quad (38)$$

With data up to only $n_{\max} = 7$, it was concluded in section 4.3 of [13] that $w \approx 6.36$ was a suitable exponent for the Bulirsch-Stoer extrapolation. It is clear from Figure 6 how this conclusion could be reached, since effectively only the the last six data points or so (we have now $n_{\max} = 14$) start bending upwards. Although this determination of Δ_2 is somewhat less accurate than (33), we are confident in concluding that $\Delta_2 = 6$ exactly.

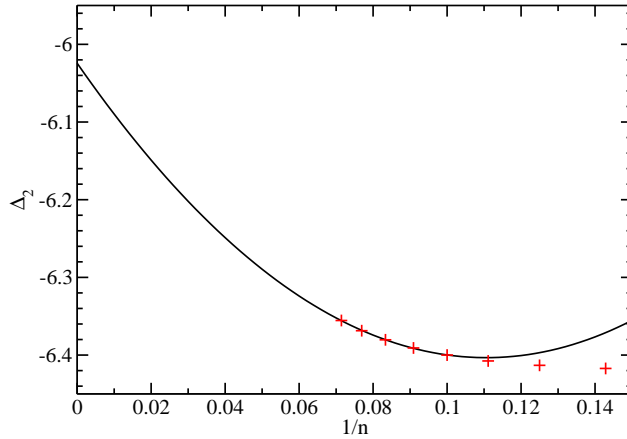


Figure 6. Determination of the leading FSS exponent Δ_2 for bond percolation on the kagome lattice.

Comparing the precisions of Δ_2 and Δ_3 obtained in section 7.1, it is clear that there is little hope of obtaining a convincing determination of Δ_3 in the present case. However, the FSS exponents Δ_k are not only a property of these lattice models of percolation, but are also expected to characterise the field theory describing their continuum limit. There is overwhelming evidence throughout the literature that both models are described, in the continuum limit, by the same conformal field theory, which can be derived by standard Coulomb gas arguments [32]. So there are good reasons to believe that we should have $\Delta_k = 2(k+1)$ also in the present case. Different lattice realisations will however give different values of the non-universal amplitudes A_k in (28). It is quite possible that the three-fold rotational symmetry of the kagome lattice (which replaces the four-fold symmetry of the square lattice) has the effect of setting $A_1 = 0$. This also matches observations made in [13].

We therefore proceed with the analysis as in section 7.1, using in particular the scaling form (34) with $A_1 = 0$. Going through the same steps as before we arrive at the final value for the percolation threshold

$$p_c = 0.524\,404\,999\,167\,439(4). \quad (39)$$

8. Connection to conformal field theory

The fact that the leading exponent in the scaling form (34) takes a high value, $\Delta_1 = 4$, is responsible for the fast convergence of $p_c(n)$ towards p_c and the ensuing precise determinations (37) and (39). We now examine how this fast convergence can be linked to considerations about the continuum limit.

The free energy per unit area $f_0(n)$ of a conformally invariant system defined on a semi-infinite cylinder of circumference n scales like [33, 34]

$$f_0(n) = f_0(\infty) - \frac{\pi c}{6n^2} + o(n^{-2}), \quad (40)$$

where c is the central charge of the corresponding conformal field theory (CFT) and $f_0(\infty)$ is the bulk free energy. This can be related to the largest eigenvalue Λ_0 of the transfer matrix for a corresponding lattice model as $f_0(n) = -\frac{\zeta}{n} \log \Lambda_0$, where ζ is a geometrical factor that depends on the lattice ($\zeta = 1$ for the square lattice) and ensures the correct normalisation per unit area in the lattice model.

Similarly, the free energy $f_i(n)$ of excited states ($i = 1, 2, \dots$) has the scaling [35]

$$f_i(n) - f_0(n) = \frac{2\pi x_i}{n^2} + o(n^{-2}), \quad (41)$$

where x_i is the corresponding scaling dimension (critical exponent). The smallest excitation $f_1(n)$ of the CFT corresponding to percolation is related to the magnetic exponent x_m , so we have $x_1 = x_m$. The values $c = 0$ and $x_m = \frac{5}{48}$ are of course known [32], but they are not important for the following argument.

The important point is that the two transfer matrix sectors, T_{open} resp. T_{closed} , considered in section 4 correspond to excitations in which an FK cluster (resp. a dual FK cluster) is required to propagate along the semi-infinite cylinder. Define now the corresponding free energies per unit area

$$f_{\text{open}}(n) = -\frac{\zeta}{n} \log \Lambda_{\text{open}}, \quad f_{\text{closed}}(n) = -\frac{\zeta}{n} \log \Lambda_{\text{closed}}. \quad (42)$$

In the continuum limit there is no difference between whether the propagating cluster is an FK cluster or a dual FK cluster. Therefore $f_{\text{open}}(n)$ and $f_{\text{closed}}(n)$ both determine the same critical exponent, namely x_m , and they both scale like $f_1(n)$ in (41). It follows that the difference

$$f_{\text{open}}(n) - f_{\text{closed}}(n) = o(n^{-2}) \quad (43)$$

vanishes fast as $n \rightarrow \infty$, right at the critical point $p = p_c$.

This is a suggestive argument, but it does not quite explain the convergence properties of the eigenvalue method. What we have observed in sections 4 and 7 is, that if we define a pseudo-critical point $p_c(n)$ as the value of p for which $f_{\text{open}}(n) - f_{\text{closed}}(n) = 0$, then

$$p_c(n) - p_c = O(n^{-4}), \quad (44)$$

and moreover the corrections appear to be $O(n^{-6})$, $O(n^{-8})$, and so on.

It is clear that more work would be required to establish whether (43) can be shown—obviously using more ingredients—to actually imply (44). But one thing that has become clear is, that the eigenvalue method owes its success to the fact that $f_{\text{open}}(n)$ and $f_{\text{closed}}(n)$ are two different ways of determining the *same* critical exponent. This will be exploited further in section 10.

9. Spin representation

It is of interest to review the definition (4) of the graph polynomial $P_B(q, v)$ when $q \in \mathbb{N}$. In that case the Potts model can be defined directly in terms of q -component spins, instead of the FK clusters that we have considered this far.

Let again the basis B consist of $n \times m$ unit cells of the lattice \mathcal{L} . Define $Z_{\mu,\nu}$ as the partition function on B with doubly periodic boundary conditions that are *twisted* by $\mu = 0, 1, \dots, q-1$ (resp. $\nu = 0, 1, \dots, q-1$) in the horizontal (resp. vertical) direction. By this we mean that the values of a pair of nearest-neighbour spins, σ_i and σ_j , that are on opposite sides of the horizontal (resp. vertical) periodic boundary condition are considered identical if $\sigma_i - \sigma_j = \mu \bmod q$ (resp. $\sigma_i - \sigma_j = \nu \bmod q$), and different otherwise.

To relate the partition functions $Z_{\mu,\nu}$ in the spin representation to those in the FK-representation (Z_{0D} , Z_{1D} and Z_{2D}) we first notice that untwisted boundary conditions are simply doubly periodic, whence

$$Z_{00} = Z_{0D} + Z_{1D} + Z_{2D}. \quad (45)$$

Consider next the quantity $\sum_{\mu,\nu} Z_{\mu,\nu}$. Configurations in Z_{0D} contribute to all q^2 terms in this sum, whereas those in Z_{2D} can only contribute to one term, namely Z_{00} . Finally, configurations in Z_{1D} are such that all clusters that are non-homotopic to a point have the same topology, i.e., they have the same winding numbers (n_x, n_y) with respect to the horizontal and vertical periodic boundary conditions [36]. These winding numbers are defined up to a global sign change, $(-n_x, -n_y) \equiv (n_x, n_y)$, and if they are both non-zero they must satisfy

$$\gcd(n_x, n_y) = 1. \quad (46)$$

Now, for a configuration in Z_{1D} to contribute to $Z_{\mu,\nu}$ we should have

$$n_x \mu + n_y \nu = 0 \bmod q. \quad (47)$$

Thanks to the constraint (46), this equation has precisely q solutions for the labels (μ, ν) . Summarising, we have proved that

$$\sum_{\mu=0}^{q-1} \sum_{\nu=0}^{q-1} Z_{\mu,\nu} = q^2 Z_{0D} + q Z_{1D} + Z_{2D}. \quad (48)$$

Combining (45) and (48) we obtain

$$Z_{00} - \frac{1}{q} \sum_{\mu=0}^{q-1} \sum_{\nu=0}^{q-1} Z_{\mu,\nu} = \left(1 - \frac{1}{q}\right) (Z_{2D} - q Z_{0D}), \quad (49)$$

so the quantity on the left-hand side is proportional to the graph polynomial $P_B(q, v)$ by (4). This was already shown in the appendix of [14], by using a more involved argument of duality transformations.

We now consider the $m \rightarrow \infty$ limit of (49) in order to obtain an eigenvalue criterion in the spin representation which is equivalent to (4). The asymptotic behaviour, as $m \rightarrow \infty$, of the partition functions reads

$$Z_{\mu,\nu} = c_{\mu,\nu} (\Lambda_\mu)^m + c_{\mu,\nu}^{(1)} (\Lambda_\mu^{(1)})^m + \dots, \quad (50)$$

where the eigenvalues depend only on μ , but the coefficients can depend on both twist labels. We have ordered the eigenvalues in decreasing order: $\Lambda_\mu > \Lambda_\mu^{(1)} > \dots$.

Moreover, the dominant eigenvalues in each sector decrease when the twist increases, $\Lambda_0 > \Lambda_1 > \dots$, where obviously $\Lambda_\mu = \Lambda_{q-\mu}$. Moreover, some of the inequalities might not be sharp when q takes particular values.

Going back to the left-hand side of (49), we see that the dominant contribution $(\Lambda_0)^m$ cancels out between the two terms. The next-leading contributions come from $\Lambda_0^{(1)}$ and Λ_1 . These must cancel out in order for $P_B(q, v)$ to vanish:

$$P_B(q, v) = 0 \quad \Leftrightarrow \quad \Lambda_0^{(1)} = \Lambda_1, \quad (51)$$

valid for finite n , in the limit $m \rightarrow \infty$. This is the spin-representation version of our main result (13).

The two eigenvalues involved have a very precise meaning. The leading eigenvalue Λ_0 in the untwisted (periodic) sector corresponds to an eigenvector which is invariant under a global permutation of the spin, $\sigma_i \rightarrow p\sigma_i$ with $p \in S_q$. The next-leading eigenvalue $\Lambda_0^{(1)}$ transforms non-trivially under such a transformation: it picks up a non-trivial q 'th root of unity. For instance, when $q = 2$, $\Lambda_0^{(1)}$ is the largest eigenvalue corresponding to an eigenvector which is odd under spin reversal. It is well-known that the free-energy gap between $\Lambda_0^{(1)}$ and Λ_0 determines the magnetic exponent x_m by (41). On the other hand, Λ_1 is the largest eigenvalue in the twisted sector $\mu = 1$, in which spin labels are shifted cyclically by one unit when one crosses the periodic boundary condition. It is equally well-known that its free-energy gap with respect to the ground state Λ_0 determines the *same* exponent x_m . It follows that the criterion (51) can be discussed in exactly the same terms as in section 8.

10. $O(N)$ loop model

The graph polynomial method, and its eigenvalue version pursued in the present paper, can be seen as a tentative to generalise the notion of self-duality to situations, where duality is not an exact symmetry. In the Potts model, a duality transformation exists directly on the lattice, and interchanging the lattice and the dual lattice amounts to shifting cyclically the sites in the loop representation by one lattice unit. This transformation provides a bijection between the states in the open and closed sectors, as discussed in section 3.

It is clearly of interest to formulate the graph polynomial method also for other models, and in particular for the $O(N)$ loop model [37, 38]. Although the two models are in the same universality class—to be more precise, the dense phase of the $O(N)$ model has the same central charge and a closely related, albeit not identical, operator content as the critical q -state Potts model with $N = \sqrt{q} = n_{\text{loop}}$ [32]—their lattice definitions present subtle differences, which were remarked early on [36]. The $O(N)$ model does not possess a duality transformation on the lattice, and it treats parity issues in a different way than the loop formulation of the Potts model. In particular, in the periodic transfer matrix formalism, the $O(N)$ model can be defined on any number of strands, whereas in the Potts model the number of strands needs to be even (e.g., there were $2n$ strands

in Figure 1). Also, on a semi-infinite cylinder with free boundary conditions at the infinities, the number of non-contractible (winding) loops in the Potts model must be even, but in the $O(N)$ model this number can have any parity.

These subtleties have some important consequences in the continuum limit, as can be seen by examining the operator content of the models in detail. Arguably the most important difference is that the energy operators of the two models do not coincide, as can be seen from a detailed Coulomb gas (CG) analysis [39, 36, 32]. The same analysis also reveals that the $O(N)$ model possesses two kinds of involutions that could be viewed as duality symmetries. The first involution exchanges the dense and dilute theories corresponding to the same central charge, by replacing the CG coupling constant g by $1/g$. The second involution originates from the study of modular invariant partition functions [40] and amount to exchanging the the role of electric and magnetic charges in the CG.

10.1. Eigenvalue method

The observations made in section 8 give us an important hint about how to obtain an eigenvalue criterion for the $O(N)$ loop model, similar to (13) and (51) for the Potts model. It seems that we should try to identify one same critical exponent that arises in the continuum limit of two topologically distinct sectors of the transfer matrix. Moreover, the introduction to section 10 provides the clue that the two sectors should differ by their charge content (i.e., electric versus magnetic) in the Coulomb gas analysis.

The algebraic framework of the $O(N)$ model is that of the dilute TL algebra. The precise setup that we shall need is that of the dilute augmented Jones-Temperley-Lieb algebra, whose description is as in section 3, except that we should now allow for dilution, in the sense that some vertices and edges are not covered by loops. To make this statement precise, we first recall that the Potts model defined on a planar graph G is equivalent [26] to a completely packed loop model defined on the 4-regular medial graph $\mathcal{M}(G)$, with the loops around a vertex of $\mathcal{M}(G)$ being in any of the two states (5). In the case of the $O(N)$ model, the loops are defined directly on the chosen graph G , which hence needs not be 4-regular [37], but to keep things simple we shall concentrate on the $O(N)$ model defined on the square lattice [38]. The two states (5) are then replaced by the following nine states of the loops around a vertex

$$\rho_1 \quad \rho_2 \quad \rho_3 \quad \rho_4 \quad \rho_5 \quad \rho_6 \quad \rho_7 \quad \rho_8 \quad \rho_9 \quad (52)$$

We define \check{R}_i as the sum over those nine diagrams, each one being weighed by the corresponding Boltzmann weight ρ_i as shown. Integrable choices of \check{R}_i exist [38] and will be discussed in section 10.2, but for the moment we are interested in the general—and not necessarily critical—case where ρ_i take arbitrary values.

In this dilute model the TL generators E_i are defined as before [see (5)], except that E_i can only be applied when the strands i and $i+1$ are occupied by loop segments,

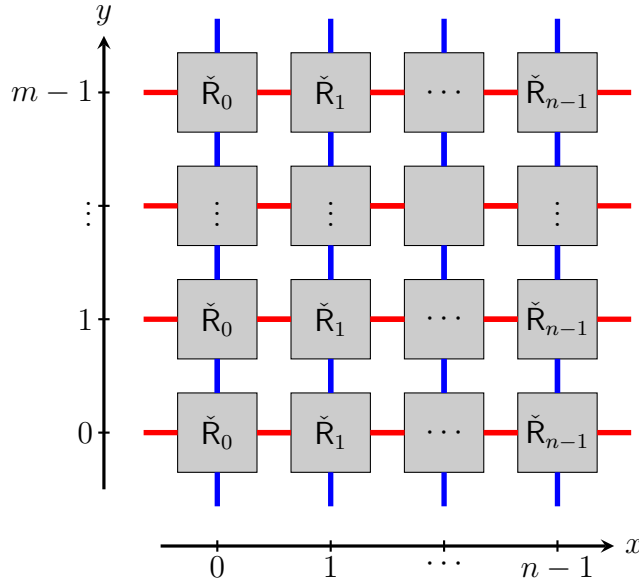


Figure 7. Transfer matrix construction in the loop representation for the $O(N)$ model. Periodic boundary conditions have been imposed horizontally. The auxiliary and quantum spaces, shown in red and blue colour respectively, sustain loops which are acted upon by an \check{R}_i -matrix inside each grey square.

corresponding to the ninth diagram in (52). The algebraic relations (7) are unchanged, but must be supplemented by the requirement that each of the nine generators (52) can act only when the loop strands have the correct occupancy. This is graphically clear, but slightly cumbersome to write down in algebraic terms [41]. Note that the weight of a closed loop is now denoted $N = n_{\text{loop}}$.

The transfer matrix T is again defined as the product over \check{R}_i , followed by a trace over the auxiliary space, as shown in Figure 7. As usual in the algebraic approach to integrable systems, the direction of time propagation is upwards in diagrams, such as (52), defining the action of algebra generators, whereas time flows to the North-East when auxiliary spaces are present. It follows that the diagrams (52) must be rotated 45° in the clockwise direction before being placed inside the gray squares in Figure 7.

The states on which T acts can still be drawn as in Figure 2, except that empty vertices are now possible (and can be represented by the special code ‘0’).

There are two types of operators in the CG. A magnetic operator $\mathbf{m}_s(r)$ inserts a topological defect, so that s oriented loop strands are created in a small neighbourhood around the point r . The two-point function $\langle \mathbf{m}_s(r_1) \mathbf{m}_{-s}(r_2) \rangle$ corresponds, in the cylinder geometry where r_1 and r_2 reside at either extremity, to imposing the propagation of s strings in the transfer matrix setup of section 3. In particular, the largest eigenvalue $\Lambda^{(s)}$ of $T^{(s)}$ [cf. (9)] determines the critical exponent x_s of the operator \mathbf{m}_s , via (41). Note that s can have any parity in the $O(N)$ model, unlike the Potts case

where $s = 2k$ must be even. If the loop weight is parameterised as

$$N = -2 \cos(\pi g), \quad (53)$$

where g is the CG coupling constant, then [32]

$$x_s = \frac{1}{8}gs^2 - \frac{(1-g)^2}{2g}. \quad (54)$$

The other type of CG operator is the electric operator $\mathbf{e}_e(r)$, also known as a vertex operator. Its key property is that the two-point function $\langle \mathbf{e}_e(r_1) \mathbf{e}_{-e}(r_2) \rangle$ amounts, in the cylinder geometry and in the $s = 0$ sector, to setting the weight of each non-contractible loop to

$$N_{\text{wind}} = 2 \cos(\pi e). \quad (55)$$

The particular choice $e = e_0 \equiv 1 - g$ corresponds to the usual situation $N_{\text{wind}} = N$, which provides the ground state of the model. The corresponding charge e_0 is called the background electric charge. For general e , the critical exponent with respect to the ground state reads [32]

$$\tilde{x}_e = \frac{e^2 - (1-g)^2}{2g}. \quad (56)$$

The dense (resp. dilute) phase of the $O(N)$ model corresponds to the regime $0 < g \leq 1$ (resp. $1 \leq g \leq 2$). The results for the dense phase also apply to the critical Potts model, by setting $N = \sqrt{q}$. In particular, setting $N_{\text{wind}} = 0$ amounts to forbidding winding loops, so—by the reasoning of sections 3 and 8—we obtain the magnetic exponent as $x_m = \tilde{x}_{1/2}$.

Motivated by the introductory remarks in this subsection, we now consider the lowest magnetic excitation \mathbf{m}_1 , corresponding to having one string propagate along the cylinder, with exponent x_1 given by (54). The electric exponent \tilde{x}_e in (56) can be made to take the same value upon making a particular choice of the charge e :

$$\tilde{x}_e - x_1 = \frac{e^2}{2g} - \frac{g}{8} = 0 \quad \Leftrightarrow \quad e = \pm \frac{g}{2}. \quad (57)$$

This is equivalent to choosing

$$N_{\text{wind}} = \pm \sqrt{2 - N}. \quad (58)$$

More generally, we would get $\tilde{x}_e = x_s$ for $e = \pm sg/2$, but taking the clue from the Potts result, we should focus on the closest equivalent of the magnetic (order parameter) operator in the Potts model, which is indeed \mathbf{m}_1 in the $O(N)$ case [39].

Based on this argument, we define the eigenvalue method for the $O(N)$ model as follows. For finite size n , find the value of the parameters $\rho_i(n)$ so that the largest eigenvalue in the $s = 1$ sector, $\Lambda^{(1)}$, coincides with the largest eigenvalue $\tilde{\Lambda}$ in the $s = 0$ sector with the particular choice (58):

$$\Lambda^{(1)} = \tilde{\Lambda}, \quad \text{with } N_{\text{wind}} = \pm \sqrt{2 - N}. \quad (59)$$

The sign ambiguity on the right-hand side will be resolved later.

This proposed method succeeds or fails depending on whether it can deliver both features that distinguished the eigenvalue method for the Potts model:

- (i) The values $\rho_i(n)$ should be *independent* of n in exactly solvable cases.
- (ii) For non-solvable cases, $\rho_i(n)$ should converge “very fast” in n .

This success criterion will be examined in details in the remainder of this section. But let us note for now one encouraging observation. The dense $O(1)$ model with vertices (52) is equivalent to a site percolation problem on the square lattice, with certain local interactions depending on ρ_i . It is known that for a particular choice of ρ_i , that corresponds to the integrable model [38] with an arbitrary inhomogeneous choice of spectral parameters, the ground state has a combinatorial nature that can be investigated [42] via the quantum Knizhnik-Zamolodchikov approach. The ground state in the $s = 1$ sector is also combinatorial, and in particular (59) holds true for any finite n , with the choice $N_{\text{wind}} = N = 1$.

10.2. Exactly solvable cases

We now consider the integrable case [38, 43] of the model (52) with weights

$$\begin{aligned}
\rho_1(u) &= 1 + \frac{\sin(u) \sin(3\lambda - u)}{\sin(2\lambda) \sin(3\lambda)}, \\
\rho_2(u) &= \rho_3(u) = \frac{\sin(3\lambda - u)}{\sin(3\lambda)}, \\
\rho_4(u) &= \rho_5(u) = \frac{\sin(u)}{\sin(3\lambda)}, \\
\rho_6(u) &= \rho_7(u) = \frac{\sin(u) \sin(3\lambda - u)}{\sin(2\lambda) \sin(3\lambda)}, \\
\rho_8(u) &= \frac{\sin(2\lambda - u) \sin(3\lambda - u)}{\sin(2\lambda) \sin(3\lambda)}, \\
\rho_9(u) &= -\frac{\sin(u) \sin(\lambda - u)}{\sin(2\lambda) \sin(3\lambda)}.
\end{aligned} \tag{60}$$

The spectral parameter u governs the anisotropy of the interactions, and we have here written $\rho_i = \rho_i(u)$ for later convenience. The crossing parameter λ is related to the loop weight via

$$N = -2 \cos(4\lambda). \tag{61}$$

We take arbitrary inhomogeneous spectral parameters, meaning that $u = u_k$ for any vertex in the k 'th column of the lattice.

For size $n = 1$ there is just one reduced state in either of the sectors $s = 0$ and $s = 1$. The one-dimensional transfer matrices $T^{(s)}$ read

$$\begin{aligned}
T^{(0)} &= \rho_1(u_1) + N_{\text{wind}} \rho_6(u_1), \\
T^{(1)} &= \rho_7(u_1) + \rho_8(u_1) + \rho_9(u_1).
\end{aligned} \tag{62}$$

Using trigonometric identities, the difference $T^{(0)} - T^{(1)}$ is proportional to $N_{\text{wind}} + 2 \cos 2\lambda$, so we conclude that (59) is satisfied with

$$N_{\text{wind}} = -2 \cos(2\lambda). \tag{63}$$

As λ goes from 0 to π , the loop weight N runs through the range $[-2, 2]$ four times, corresponding to the four branches of critical behaviour discussed in [38]. The first two branches, $\lambda \in [0, \frac{\pi}{4}]$ and $\lambda \in [\frac{\pi}{4}, \frac{\pi}{2}]$, correspond to the dilute and dense phase, respectively. The relation between (61) and (63) is such that the plus (resp. minus) sign in front of the square root in (59) should be taken for $\lambda \in [\frac{\pi}{4}, \frac{3\pi}{4}]$ (resp. $\lambda \in [0, \frac{\pi}{4}] \cup [\frac{3\pi}{4}, \pi]$). In particular, the plus (resp. minus) sign should be taken for the dense (resp. dilute) phase of the $O(N)$ model.

We now seek confirmation of these results for size $n = 2$. In the sector $T^{(0)}$ there are 3 reduced states which can be written $\circ\circ$, $()$ and $)()$, where \circ denotes an empty site, and the remainder of the notation is as in section 4.1. In the sector $T^{(1)}$ the 2 reduced states are $|\circ$ and $\circ|$. With this ordering of the bases, the transfer matrices read

$$T^{(0)} = \begin{bmatrix} \rho_1\rho'_1 + \rho_6\rho'_6\tilde{N} & \rho_3\rho'_4N + \rho_4\rho'_3\tilde{N} & \rho_3\rho'_4\tilde{N} + \rho_4\rho'_3N \\ \rho_5\rho'_2 & \rho_7\rho'_7 + \rho_9\rho'_8\tilde{N} & \rho_8\rho'_8 + \rho_9\rho'_9 + \rho_9\rho'_8N \\ \rho_2\rho'_5 & \rho_8\rho'_8 + \rho_9\rho'_9 + \rho_8\rho'_9N & \rho_7\rho'_7 + \rho_8\rho'_9\tilde{N} \end{bmatrix} \quad (64)$$

and

$$T^{(1)} = \begin{bmatrix} \rho_7\rho'_1 + \rho_8\rho'_6 + \rho_9\rho'_6 & \rho_2\rho'_3 + \rho_5\rho'_4 \\ \rho_3\rho'_2 + \rho_4\rho'_5 & \rho_1\rho'_7 + \rho_6\rho'_8 + \rho_6\rho'_9 \end{bmatrix}, \quad (65)$$

where we have abbreviated $\rho_i(u_1) = \rho_i$, $\rho_i(u_2) = \rho'_i$ and $N_{\text{wind}} = \tilde{N}$. Inserting now (60), (61) and (63) we find that the two eigenvalues of $T^{(1)}$ coincide with two of the eigenvalues of $T^{(0)}$, for arbitrary values of the parameters λ , u_1 and u_2 .

We have similarly studied this model at size $n = 3$, in which case $\dim(T^{(0)}) = 7$ and $\dim(T^{(1)}) = 6$. Remarkably, we found that with arbitrary inhomogeneous spectral parameters, u_1 , u_2 and u_3 , and for arbitrary values of λ , all 6 eigenvalues of $T^{(1)}$ were also eigenvalues of $T^{(0)}$.

The dimensions of these transfer matrices are related to the Motzkin numbers. Define $M(x) = (1+x)(1-3x)$ and consider the generating functions

$$\begin{aligned} f_0(x) &= \frac{1}{\sqrt{M(x)}} = \sum_{n=0}^{\infty} a_n x^n, \\ f_1(x) &= \frac{2x}{M(x) + (1-x)\sqrt{M(x)}} = \sum_{n=1}^{\infty} b_n x^n. \end{aligned} \quad (66)$$

Then $a_n = \dim(T^{(0)})$ and $b_n = \dim(T^{(1)})$ for a system of size n loop strands. We have $a_n > b_n$ for $n > 1$. However, both numbers exhibit the same asymptotic behaviour for $n \gg 1$:

$$a_n \sim b_n \sim \frac{1}{2} \left(\frac{3}{\pi n} \right)^{1/2} 3^n. \quad (67)$$

We conjecture that with inhomogeneous spectral parameters, *all* eigenvalues of $T^{(1)}$ are also eigenvalues of $T^{(0)}$, provided the weight of non-contractible loops is taken as in (63). If true, this would be very promising for finding a genuine graph polynomial for the $O(N)$ model, i.e., one having properties similar to those of $P_B(q, v)$ in the Potts case

[10, 12, 13] for *finite* $n \times m$ bases, and not just in the $m \rightarrow \infty$ limit. We hope to report more on this soon.

10.3. Approximation method

We now investigate the second aspect of the eigenvalue method for the $O(N)$ model, namely its usefulness as an approximation method for the critical points of non-solvable models. To this end, we apply it to the problem of self-avoiding polygons (SAP) on the square lattice, which is the $N \rightarrow 0$ limit of a loop model in which each occupied edge has the weight z . There is no bending rigidity, and the osculating vertices ρ_8 and ρ_9 are disallowed. The Boltzmann weights (52) are thus

$$\begin{aligned}\rho_1 &= 1, \\ \rho_2 &= \rho_3 = \rho_4 = \rho_5 = \rho_6 = \rho_7 = z, \\ \rho_8 &= \rho_9 = 0.\end{aligned}\tag{68}$$

Note that we have suppressed the spectral parameter u , since this model is not integrable.

This SAP model has been extensively studied by exact enumeration techniques [18, 19, 20], and the critical monomer fugacity is known to very high precision [21]

$$z_c = 0.379\,052\,277\,752(3).\tag{69}$$

This value corresponds to the smallest $z > 0$ for which the generating function, as obtained by exact enumeration, exhibits a singularity. In the formulation of the problem in terms of a partition function, with the weights (68), this corresponds to selecting the dilute branch of the $O(N)$ model, and implies taking the minus sign in (59). We therefore set $N = 0$ and $N_{\text{wind}} = -\sqrt{2}$.

By diagonalising the transfer matrices $T^{(0)}$ and $T^{(1)}$ and proceeding as in section 5, we have obtained values of $z_c(n)$ up to $n_{\text{max}} = 19$ for the SAP problem. They are shown in Table 5. It is clear that these data exhibit the required fast convergence, and a detailed analysis—to be presented elsewhere [22]—reveals that the scaling is in fact compatible with (34).

We should emphasise that the formulation in terms of a partition function allows us to study the problem (68) also for other values of N , and in the dense phase. The dilute $N = 1$ case corresponds to an Ising model on the square lattice in which configurations of alternating spins $(+ - + - \text{ or } - + - +)$ around a lattice face have been disallowed, since we have set $\rho_8 = \rho_9 = 0$. This produces a value of the critical domain wall fugacity, $z_c = 0.421\,326 \dots$, which is slightly lower than that of the standard Ising model, which reads $z_c^{\text{Ising}} = (1 + \sqrt{2})^{-1} = 0.414\,214 \dots$.

The *dense* phase of SAP (with $N = 0$) does not appear to have been studied explicitly within the exact enumeration framework, but the corresponding z_c is likely to manifest itself as a subdominant singularity of standard, dilute SAP.

n	$z_c(n)$
2	0.3832870437289217825415444959209990643484
3	0.3800152822923947541103727449094743052839
4	0.3793419092420152604076859124268482909456
5	0.3791615386298805591124869699564102732536
6	0.3791017465104568577033096312174651793134
7	0.3790779263723816763857349117326710080035
8	0.3790669419366251682820022783255996752011
9	0.3790612863965732376129739341339159714858
10	0.3790581237478262657302859193323348704028
11	0.3790562392439348634338963536547147709970
12	0.3790550583590770828697993099179842253186
13	0.3790542873705249946097446478792002255473
14	0.3790537664746062070854620937409756594548
15	0.3790534041836437725305420784870138649786
16	0.3790531458388626510867578645132848654379
17	0.3790529575762840825464391257666224019613
18	0.3790528177462476184521578790271596607432
19	0.3790527121228867470
Ref. [21]	0.379052277752 (3)

Table 5. Critical fugacities $z_c(n)$ of the SAP model on the square lattice, as computed from $n \times \infty$ bases, and a previous result for z_c .

We finally note that when applying (59) to a non-solvable model, the parameter $z_c(n)$ can indeed be tuned so that the leading eigenvalues of $T^{(0)}$ and $T^{(1)}$ coincide, but the remaining eigenvalues of $T^{(1)}$ will in general not be equal to eigenvalues of $T^{(0)}$.

11. Discussion

In this paper we have transformed the graph polynomial method of [10, 12, 13] into an eigenvalue method. This corresponds formally to taking the $m \rightarrow \infty$ limit of the $n \times m$ bases B that enter the definition of the graph polynomial P_B . The advantages of this reformulation are numerous and have been discussed in the Introduction. We can add to this list that, on a technical level, the eigenvalue method requires only the reduced states in the transfer matrix setup (see section 3) and avoids the rather complicated topological considerations of [13] (see section 3.7 of that reference in particular), two facts that make the practical implementation of the method considerably easier.

On a more fundamental level, the eigenvalue formulation has revealed that the method hinges on identifying two distinct topological sectors of the transfer matrix that lead to the determination of one same critical exponent. This has enabled us to extend the applicability of the method from the q -state Potts model—including bond

and site percolation problems—to encompass $O(N)$ models in various phases, even in the presence of inhomogeneities. Also in the $O(N)$ case we have demonstrated that the method is both capable of

- (i) detecting exact solvability (in the sense that integrable models lead to results independent of the size n), and of
- (ii) generating approximations to the critical parameters that converge rapidly in n .

This first aspect poses a set of fundamental questions that should motivate future research. In particular, the possible link between exact factorisation in the graph polynomial method and discrete holomorphicity (alias conservation of non-local currents in quantised affine algebras [3, 4]), or related manifestations of exact solvability, remains to be elucidated. With the present extension from Potts to $O(N)$ models, we have demonstrated that the graph polynomial method is likely to be as ubiquitous and versatile as discrete holomorphicity. The fact that the $O(N)$ version of the method required us to impose a very particular value of N_{wind} in (59), and the ensuing massive eigenvalue coincidences between $T^{(1)}$ and $T^{(0)}$, are strongly reminiscent of phenomena encountered in representation theory [44], and this possible link should be examined as well.

The second aspect has enabled us to study the finite-size scaling properties of the method in much more detail than [13]. In particular, we have developed powerful extrapolation schemes capable of determining the critical point to within 15-digit precision. In future work, we plan to extend these determinations to other lattices (following [13] in the Potts case), and to other values of the parameters q and N . From a more practical perspective, we are working on a parallel implementation of the algorithm which should make accessible larger n and lead to even higher precision [25].

Finally, the extension to yet other models, such as Z_N models and multi-coloured loops, previously considered from the discrete holomorphicity perspective [5, 9], should also be investigated. The question of whether the present method applies to loop models with non-trivial boundary interactions [45, 46, 47] provides another appealing perspective.

Acknowledgments

This work was supported by the Agence Nationale de la Recherche (grant ANR-10-BLAN-0414: DIME) and the Institut Universitaire de France. The author warmly thanks A.J. Guttmann, M. Ohzeki and C.R. Scullard for discussions and collaboration on related subjects, and A.D. Sokal for the kind permission to use computational resources (provided by Dell Corporation) at New York University. He is also grateful for the hospitality of the Centre of Excellence for Mathematics and Statistics of Complex Systems (Melbourne University) and the Galileo Galilei Institute of Theoretical Physics (Arcetri, Florence) where part of this work was accomplished.

References

- [1] Baxter R J 1982 *Exactly solved models in statistical mechanics* (Academic Press, London)
- [2] Cardy J 2009 *J. Stat. Phys.* **137** 814
- [3] Bernard D and Felder G 1991 *Nucl. Phys. B* **365** 98
- [4] Ikhlef Y, Weston R, Wheeler M and Zinn-Justin P 2013 *J. Phys. A: Math. Theor.* **46** 265205
- [5] Rajabpour M A and Cardy J 2007 *J. Phys. A: Math. Theor.* **40** 14703
- [6] Riva V and Cardy J 2006 *J. Stat. Mech.* P12001
- [7] Ikhlef Y and Cardy J 2009 *J. Phys. A: Math. Theor.* **42** 102001
- [8] Ikhlef Y and Weston R 2015 *arXiv:1502.04944*
- [9] Ikhlef Y, Fendley P and Cardy J 2011 *Phys. Rev. B* **84** 144201
- [10] Jacobsen J L and Scullard C R 2012 *J. Phys. A: Math. Theor.* **45** 494003
- [11] Scullard C R and Jacobsen J L 2012 *J. Phys. A: Math. Theor.* **45** 494004
- [12] Jacobsen J L and Scullard C R 2013 *J. Phys. A: Math. Theor.* **46** 075001
- [13] Jacobsen J L 2014 *J. Phys. A: Math. Theor.* **47** 135001
- [14] Ohzeki M and Jacobsen J L 2015 *J. Phys. A: Math. Theor.* **48** 095001
- [15] Wu F Y 1979 *J. Phys. C* **12** L645
- [16] Ziff R M and Suding P N 1997 *J. Phys. A: Math. Gen.* **30** 5351
- [17] Feng X, Deng Y and Blöte H W J 2008 *Phys. Rev. E* **78** 031136
- [18] Enting I G 1980 *J. Phys. A: Math. Gen.* **13** 3713
- [19] Conway A R, Enting I G and Guttmann A J 1993 *J. Phys. A: Math. Gen.* **26** 1519
- [20] Jensen I and Guttmann A J 1999 *J. Phys. A: Math. Gen.* **32** 4867
- [21] Clisby N and Jensen I 2012 *J. Phys. A: Math. Theor.* **45** 115202
- [22] Guttmann A J, Jacobsen J L, Jensen I and Scullard C R 2015 *in preparation*
- [23] Potts R B 1952 *Proc. Camb. Phil. Soc.* **48** 106
- [24] Fortuin C M and Kasteleyn P W 1972 *Physica* **57** 536
- [25] Jacobsen J L and Scullard C R 2015 *in preparation*
- [26] Baxter R J, Kelland S B and Wu F Y 1976 *J. Phys. A: Math. Gen.* **9** 397
- [27] Temperley H N V and Lieb E H 1971 *Proc. R. Soc. London A* **322** 251
- [28] Gainutdinov A M, Read N, Saleur H and Vasseur R 2015 *JHEP* **05** 114
- [29] Richard J F and Jacobsen J L 2006 *Nucl. Phys. B* **750** 250–264
- [30] Richard J F and Jacobsen J L 2007 *Nucl. Phys. B* **769** 256–274
- [31] Saad Y 2000 *Iterative methods for sparse linear systems* 2nd ed (SIAM)
- [32] Jacobsen J L 2009 Conformal field theory applied to loop models, *in* Polygons, polyominoes and polycubes, *Lecture Notes in Physics* vol **775** ed Guttmann A J (Heidelberg: Springer Verlag) pp 347–424
- [33] Blöte H W J, Cardy J L and Nightingale M P 1986 *Phys. Rev. Lett.* **56** 742
- [34] Affleck I 1986 *Phys. Rev. Lett.* **56** 746
- [35] Cardy J L 1984 *J. Phys. A: Math. Gen.* **17** L385
- [36] DiFrancesco P, Saleur H and Zuber J B 1987 *J. Stat. Phys.* **49** 57
- [37] Nienhuis B 1982 *Phys. Rev. Lett.* **49** 1062
- [38] Blöte H and Nienhuis B 1989 *J. Phys. A: Math. Gen.* **22** 1415
- [39] Nienhuis B 1984 *J. Stat. Phys.* **34** 731
- [40] DiFrancesco P, Saleur H and Zuber J B 1987 *Nucl. Phys. B* **285** 454
- [41] Grimm U and Pearce P A 1993 *J. Phys. A: Math. Gen.* **26** 7435
- [42] Garbali A and Nienhuis B 2014 *arXiv:1411.7020*
- [43] Zhou Y and Batchelor M 1997 *Nucl. Phys. B* **485** 646
- [44] Gainutdinov A, Jacobsen J L, Read N, Saleur H and Vasseur R 2013 *J. Phys. A: Math. Theor.* **46** 494012
- [45] Jacobsen J L and Saleur H 2008 *Nucl. Phys. B* **788** 137
- [46] Dubail J, Jacobsen J L and Saleur H 2009 *Nucl. Phys. B* **813** 430

- [47] Dubail J, Jacobsen J L and Saleur H 2010 *Nucl. Phys. B* **827** 457